Journal of Alloys and Compounds 809 (2019) 151773

Contents lists available at ScienceDirect

Journal of Alloys and Compounds

journal homepage: http://www.elsevier.com/locate/jalcom

Structural, elastic, electronic and vibrational properties of XAl_2O_4 (X = Ca, Sr and Cd) semiconductors with orthorhombic structure

S. Akbudak [a, *], A. Candan [b], A.K. Kushwaha [c], A.C. Yadav [c], G. Uğur [d], Ş. Uğur [d]

[a] Department of Physics, Faculty of Arts and Sciences, Adiyaman University, 02100, Adiyaman, Turkey
[b] Department of Machinery and Metal Technology, Ahi Evran University, 40100, Kırşehir, Turkey
[c] Department of Physics, K.N. Govt. P.G. College, Gyanpur, Bhadohi, 221304, India
[d] Department of Physics, Faculty of Science, Gazi University, 06500, Ankara, Turkey

ARTICLE INFO

Article history:
Received 11 May 2019
Received in revised form
6 August 2019
Accepted 8 August 2019
Available online 8 August 2019

Keywords:
Orthorhombic structure
Semiconductor
Elastic constants
Phonon dispersion curves

ABSTRACT

Structural, elastic, electronic and vibrational properties of XAl_2O_4 (X = Ca, Sr and Cd) compounds with orthorhombic structure are studied by first principles method within generalized gradient approximation. The calculated negative formation enthalpy for each compounds indicates the thermodynamical stability of the studied phase. Band structure calculations reveal that $CaAl_2O_4$, $SrAl_2O_4$ and $CdAl_2O_4$ compounds have a direct band gap of 4.86, 4.54 and 2.46 eV, respectively. Besides, from the analysis of the band gap values, one can notice that the replacement of Ca atoms by Sr and Cd atoms in these compounds reduces the band gap energy values. It is also observed that the $CaAl_2O_4$, $SrAl_2O_4$ and $CdAl_2O_4$ compounds are less compressible along b-axis and their compressibility decreases in the sequence $SrAl_2O_4 > CdAl_2O_4 > CaAl_2O_4$. Similarly, it is also noticeable that the $CaAl_2O_4$ compound have more resisting power against the monoclinic shear distortion along {100} plane and along {110} direction compared to $CdAl_2O_4$ and $SrAl_2O_4$ compounds. Moreover, Cauchy pressures confirm that the $CaAl_2O_4$ and $SrAl_2O_4$ compounds are ductile while the $CdAl_2O_4$ compound is brittle in nature. This fit very well with the forecast from B/G relation. The calculated elastic constants and the phonon dispersion relations of the studied compounds show that these compounds are both mechanically and dynamically stable. Moreover the temperature dependence of the specific heat and entropy have been discussed in detail and calculated Debye temperature is in good agreement with the related study in literature.

1. Introduction

AB_2O_4 type aluminate compounds have been the main subject of many scientific studies because of their physical properties such as high reflectivity, high melting point, high strength and high chemical resistivity at high temperatures in addition to low electrical loss [1,2]. Besides, aluminates are environmentally friendly, more chemically stable and they can be easily manufactured cost-effectively [3]. Thus, the studies on the preparation and characterization of aluminate based phosphors are increasing day by day. Nowadays, many investigators are performing inquiry in seek for appropriate host lattices that can be used to arrange phosphors for solid state lighting. Aluminate-based phosphors are utilized in various technologies like plasma, surface conduction electron displays and field emission [4–6]. Inorganic phosphorus materials with high colour purity and density find use in a wide range of applications, including light-emitting diodes and imaging devices as well [7–9].

Many studies have been carried out on AB_2O_4 compounds with $CaFe_2O_4$ type orthorhombic structure so far [10–19]. Especially, monocalcium aluminates [20–30] have been the subject of many investigations, for it is the main phase in calcium aluminate cements (CAC). Calcium aluminate cements have been successfully used as linings and coatings in wastewater applications [31]. Besides, they have numerous advantages compared to traditional portland cement system. These advantages are rapid strength gain, high resistance to acid attack, high thermal resistance, minimized CO_2 emissions during fabricating, high dimensional uniformity and high abrasion resistance [32,33]. On the other hand, after being doped with a trivalent alkaline-earth metal, Eu^{3+} monocalcium aluminate can be used to produce garish pigments which exceeds a few times the luminescence properties of ZnS based classical

* Corresponding author.
E-mail address: sakbudak@adiyaman.edu.tr (S. Akbudak).

https://doi.org/10.1016/j.jallcom.2019.151773
0925-8388/

materials [34,35]. However, $CaAl_2O_4$ is also attractive from a crystal chemist point of view: Reid and Ringwood [20] as well as Ito and co-workers [21] after their initial investigations, observed that $CaAl_2O_4$ undergoes several structural phase transitions as a function of pressure and temperature. Additionally, Akaogi et al. [22] reported some extinguishable high pressure change of X-ray diffraction model. They showed that one of this phases have similar structural relation with $CaFe_2O_4$ structure. In addition, the raman spectroscopy and specific heat calculations of $CaAl_2O_4$ were performed by Kojitani et al. [23]. In another study that was carried out by Lazic and co-workers in 2006 [24], lattice parameters of *Pnma* phase $CaAl_2O_4$ ($a = 8.92004$ Å, $b = 2.87129$ Å, $c = 10.31550$ Å, $V = 264.203$ Å^3, $d = 3.973$ g cm^{-3}) were obtained using Cu-K_α radiation in X-ray diffractometer. They also investigated the crystal structure of a high pressure polymorph of hexagonal $CaAl_2O_4$ using X-ray powder diffraction data in a different study [25]. Eremin and co-workers [26] have recently calculated the crystal structure geometry, interatomic distances, phase density and elastic properties of $CaAl_2O_4$ under 200 GPa using a semi-experimental and ab initio theoretical study. In Open Quantum Material Database records [27], lattice parameters and formation enthalpy for *Pnma* phase of $CaAl_2O_4$ compound are $a = 8.896$ Å, $b = 2.874$ Å, $c = 10.307$ Å, $\Delta H_f = -3.250$ eV/atom. Similarly, in Materials Project records [28], lattice parameters and formation enthalpy for the same phase are $a = 9.000$ Å, $b = 2.900$ Å, $c = 10.411$ Å, $V = 271.685$ Å^3, $d = 3.86$ g cm^{-3}, $\Delta H_f = -3.408$ eV/atom.

When it comes to $CdAl_2O_4$, there are only a few studies related to its cubic spinel phase. Viñuela et al. [36] have obtained $CuAl_2O_4$ and cadmium including $Cd_xCu_{1-x}Al_2O_4$ compound at 1223 K from the reaction of CuO, CdO and Al_2O_3 alloys. From the theoretical side, Bouhamadou et al. [37] calculated the structural, electronic, optical and thermodynamic properties of cubic spinel $CdAl_2O_4$ using full potential linearized augmented plane wave (FP-LAPW) based density functional theory method. Also, Manzar et al. [38] have investigated the electronic and optical properties of cubic CdX_2O_4 (X = In, Ga, Al) spinels by a modified Becke-Johnson potential.

In different studies, it has been shown that rare earth doped aluminium based compounds offer strong luminescence properties [39–43]. In particular, $SrAl_2O_4$ shows great functionality as luminescent material. These types of materials can be used in various fields such as display devices, signage, medical applications and storage devices [44]. So, it is noteworthy to mention studies about $SrAl_2O_4$. Nazarov et al. [44] have investigated the changes in structural and electronic properties of $SrAl_2O_4$ after being doped with Eu^{2+} by means of density functional theory. They observed a band gap of 4.52 eV for $SrAl_2O_4$ which is underestimated compared to experimental value of 6.5 eV. The luminescence properties of nanocrystalline monoclinic $SrAl_2O_4$ with compustion synthesis method have been investigated by Fu et al. [45]. Besides, they also reported a band gap value of 4.479 eV for $SrAl_2O_4$ using full potential linearized augmented plane wave method (FP-LAPW) within density functional theory.

Zhai et al. [46] have investigated the photoluminescence properties of Tb-doped $SrAl_2O_4$ via sol-gel combustion method and the structure of this compound was verified using X-Ray Diffraction (XRD) technique. In another study, Rojas-Hernandez et al. have studied the structural properties of the $P2_1$, $P6_322$ and $P6_3$ phases of $SrAl_2O_4$ using both LDA and GGA methods [47]. Compared to large numbers of theoretical and experimental studies about $CaAl_2O_4$ available in literature, studies related to $SrAl_2O_4$ and $CdAl_2O_4$ are less frequent. Recently, hexagonal structure of XAl_2O_4 (X = Ca, Sr and Cd) has been investigated by our group [48]. However, a comprehensive density functional theory calculation for orthorhombic XAl_2O_4 (X = Ca, Sr and Cd) is missing.

So, the main purpose of this paper is to gain deep insight into the elastic, electronic, vibrational and thermodynamic properties of XAl_2O_4 (X = Ca, Sr and Cd). To attain this purpose we took advantage of the first principles density functional theory calculations.

2. Computational method

First principles density functional theory calculations are performed using MedeA code [49,50]. To carry out calculations Projected augmented wave (PAW) pseudo-potentials [51,52] together with generalized gradient approximation implemented by Perdew et al. (GGA-PBE) [53] are used. The Brillouin zone is integrated using Monkhorst-Pack generated sets of **k**-points [54]. To obtain the desired convergence, $3 \times 8 \times 2$ **k**-points for $CaAl_2O_4$ and $CdAl_2O_4$, and $3 \times 8 \times 3$ **k**-points for $SrAl_2O_4$ found to be sufficient. A kinetic energy cutoff of 532 eV for $CaAl_2O_4$ and $CdAl_2O_4$ and 554 eV for $SrAl_2O_4$ with a threshold of 10^{-5} eV is used to obtain the desired convergence. The elastic properties of the studied materials are calculated through the MT module of MedeA [55]. And phonon properties are investigated by direct method [56].

3. Results and discussion

3.1. Structural parameters

Ground state properties of any material can be obtained by calculating its structural parameters. The XAl_2O_4 (X = Ca, Sr and Cd) compounds have a $CaFe_2O_4$-type crystal structure (*Pnma*). X, Al, and O atoms occupy the 4c (x, 1/4, z) Wyckoff positions where Al and O atoms have two and four different 4c Wyckoff positions, respectively. The structural parameters of the orthorhombic XAl_2O_4 (X = Ca, Sr and Cd) compounds have been calculated using ab-initio technique within generalized gradient approximations. The calculated structural parameters for the studied compounds are given in Table 1 together with the related literature. Additionally, the obtained equilibrium atomic coordinates of the XAl_2O_4 (X = Ca, Sr and Cd) compounds in P*nma* phase are listed in Table 2. Crystal structure based on the calculated positional structures of XAl_2O_4 (X = Ca, Sr and Cd) compounds is shown in Fig. 1. Obtained results are in good agreement with the related literature [20–22,24,26–28].

On the other hand, the formation enthalpy is a significant parameter which determines the thermodynamical stability and the probability of experimental synthesis [57–59] of the compound. The formation enthalpy of XAl_2O_4 (X = Ca, Sr and Cd) compounds with orthorhombic (*Pnma*) phase has been tabulated in Table 1 with the existing results [26–28]. The formation enthalpy can be expressed with the following mathematical equation for these materials,

Table 1
Calculated lattice parameters (a, b and c in Å), volume (V in Å^3) and formation enthalpy (ΔH_f in eV/atom) of the XAl_2O_4 (X = Ca, Sr and Cd) compounds for orthorhombic (*Pnma*) phase.

Compound	Lattice parameters			V	ΔH_f	References
	a	b	c			
$CaAl_2O_4$	8.999	2.899	10.412	271.660	−3.012	Present
	8.925	2.871	10.308	264.1	–	[20-Exp.]
	8.89	2.87	10.30	263	–	[21-Exp.]
	8.923	2.872	10.306	264.09	–	[22-Exp.]
	8.920	2.871	10.316	264.203	–	[24-Exp.]
	8.911	2.852	10.395	264.19	−3.388	[26-Exp.]
	8.978	2.888	10.388	269.65	–	[26]
	8.896	2.874	10.307	–	−3.250	[27]
	9.000	2.900	10.411	271.685	−3.408	[28]
$SrAl_2O_4$	9.326	2.941	10.696	293.349	−2.885	Present
$CdAl_2O_4$	9.020	2.888	10.477	272.893	−2.392	Present

Table 2
Atomic positions of the XAl_2O_4 (X = Ca, Sr and Cd) compounds for orthorhombic (*Pnma*) phase.

Compound	Atom	x	y	z
$CaAl_2O_4$	Ca	0.2422	0.2500	0.6555
	[24-Exp.]	0.2424	0.2500	0.6562
	Al1	0.0813	0.2500	0.3971
	[24-Exp.]	0.0817	0.2500	0.3973
	Al2	0.5617	0.2500	0.6110
	[24-Exp.]	0.5628	0.2500	0.6099
	O1	0.0774	0.2500	0.0719
	[24-Exp.]	0.0774	0.2500	0.0706
	O2	0.2969	0.2500	0.3462
	[24-Exp.]	0.2966	0.2500	0.3461
	O3	0.3857	0.2500	0.0196
	[24-Exp.]	0.3846	0.2500	0.0188
	O4	0.4735	0.2500	0.7846
	[24-Exp.]	0.4727	0.2500	0.7851
$SrAl_2O_4$	Sr	0.2431	0.2500	0.6571
	Al1	0.0779	0.2500	0.3988
	Al2	0.5635	0.2500	0.6065
	O1	0.0696	0.2500	0.0726
	O2	0.2994	0.2500	0.3562
	O3	0.3902	0.2500	0.0149
	O4	0.4738	0.2500	0.7864
$CdAl_2O_4$	Cd	0.2422	0.2500	0.6553
	Al1	0.0829	0.2500	0.3968
	Al2	0.5614	0.2500	0.6129
	O1	0.0760	0.2500	0.0703
	O2	0.2970	0.2500	0.3493
	O3	0.3878	0.2500	0.0189
	O4	0.4727	0.2500	0.7849

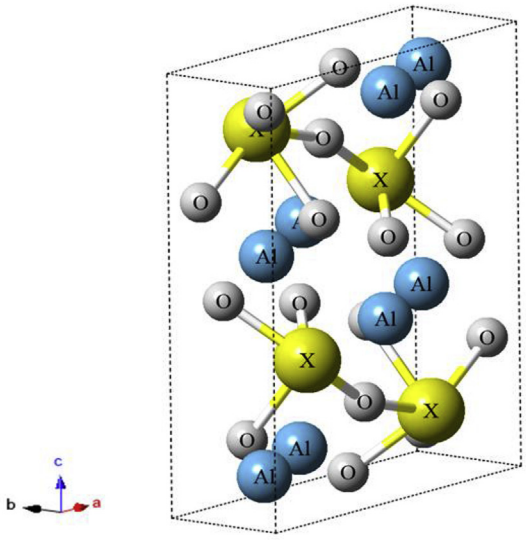

Fig. 1. (Colour online) Crystal structure of orthorhombic XAl_2O_4 (X = Ca, Sr and Cd) compounds. (For interpretation of the references to color in this figure legend, the reader is referred to the Web version of this article.)

$$\Delta H_f = E^{total}_{X_lAl_mO_n} - \left[l.E^{bulk}_X + m.E^{bulk}_{Al} + n.E^{bulk}_O\right] \quad (1)$$

where $E^{total}_{X_lAl_mO_n}$ is the equilibrium total energy of the compound, E^{bulk}_X, E^{bulk}_{Al}, and E^{bulk}_O are the individual energies of bulk structures of the X (Ca, Sr, Cd), Al and O atoms, respectively. The calculated negative formation enthalpy values of the $CaAl_2O_4$, $SrAl_2O_4$ and $CdAl_2O_4$ are −3.012, −2.885, and −2.392 eV/atom, respectively. As a result, these compounds are thermodynamically stable and may be synthesized experimentally.

3.2. Elastic constants and related properties

The complete elastic properties of the orthorhombic structure with space group *Pnma* is described by nine elastic constants C_{11}, C_{12}, C_{13}, C_{22}, C_{23}, C_{33}, C_{44}, C_{55} and C_{66}, respectively. All these elastic constants for the studied compounds are obtained by first principles method and results are given in Table 3. Elastic compliance constants (S_{ij}) for the orthorhombic XAl_2O_4 (X = Ca, Sr and Cd) compounds are also calculated and results are listed in Table 3. In the literature, since there is no data about elastic constants and elastic compliance constants of these compounds, we could not compare our results. From Table 3, it is clearly seen that the obtained elastic constants C_{11}, C_{12}, C_{13}, C_{22}, C_{23}, C_{33}, C_{44}, C_{55} and C_{66} for the XAl_2O_4 (X = Ca, Sr and Cd) compounds verify the Born's stability condition for orthorhombic structure [60];

$$C_{ii} > 0, (i = 1, 2, 3, 4, 5 \text{ and } 6), (C_{11} + C_{22} - 2C_{12}) > 0 \quad (2)$$

$$(C_{11} + C_{33} - 2C_{13}) > 0, (C_{22} + C_{33} - 2C_{23}) > 0 \quad (3)$$

$$(C_{11} + C_{22} + C_{33} + 2C_{12} + 2C_{13} + 2C_{23}) > 0 \quad (4)$$

$$(C_{11} + C_{22} + C_{33}) > 3B > (C_{12} + C_{13} + C_{23}) > 0 \quad (5)$$

Therefore, it can be inferred that studied $CaAl_2O_4$, $SrAl_2O_4$ and $CdAl_2O_4$ compounds with orthorhombic structure are mechanically stable.

C_{11}, C_{22} and C_{33} represent the resistance against linear compression along *a*-, *b*-, and *c*-directions, respectively. In the present study, the elastic constant C_{22} is greater than the other two elastic constants C_{11} and C_{33} for XAl_2O_4 (X = Ca, Sr and Cd). Thus $CaAl_2O_4$, $SrAl_2O_4$ and $CdAl_2O_4$ compounds are less compressible along *b*-axis. It is also noteworthy to mention that the compressibility along *b*-axis decreases in the sequence $CaAl_2O_4 > CdAl_2O_4 > SrAl_2O_4$. The elastic constant C_{44} represents the resistance against the monoclinic shear distortion along {100} plane. Moreover, C_{44} is also indirectly related to the hardness of the materials. However, the elastic constant C_{66} represents the resistance against shear in the {110} direction. In the present study, it is observed that the $CaAl_2O_4$ compound have more resisting power against the monoclinic shear distortion along {100} plane and more resistance against shear along {110} direction than the other two $CdAl_2O_4$ and $SrAl_2O_4$ compounds.

Table 3
Calculated elastic constants (C_{ij} in GPa) and elastic compliance constants (S_{ij}, in × $1000GPa^{-1}$) for XAl_2O_4 (X = Ca, Sr and Cd).

Compound	$CaAl_2O_4$	$SrAl_2O_4$	$CdAl_2O_4$
C_{11}	328.56	258.00	313.57
C_{12}	70.35	72.93	100.63
C_{13}	111.06	117.97	130.66
C_{22}	403.81	370.91	400.86
C_{23}	95.69	101.99	105.79
C_{33}	349.51	262.92	343.03
C_{44}	131.27	115.32	107.71
C_{55}	123.63	113.52	94.24
C_{66}	112.06	100.99	84.29
S_{11}	3.4597	4.9299	3.9383
S_{12}	−0.3660	−0.4042	−0.6453
S_{13}	−0.9991	−2.0552	−1.3010
S_{22}	2.6869	3.0511	2.8214
S_{23}	−0.6194	−1.0022	−0.6243
S_{33}	3.3482	5.1144	3.6032
S_{44}	7.6181	8.6717	9.2842
S_{55}	8.0887	8.8087	10.6111
S_{66}	8.9238	9.9019	11.8645

Taking advantage of the calculated elastic constants for XAl_2O_4 (X = Ca, Sr and Cd) compounds, bulk modulus B, shear modulus G and Young's modulus E have been obtained using the Voigt [61] approximation;

$$B_V = \frac{C_{11} + C_{22} + C_{33} + 2(C_{12} + C_{13} + C_{23})}{9} \quad (6)$$

$$G_V = \frac{C_{11} + C_{22} + C_{33} + 3(C_{44} + C_{55} + C_{66}) - C_{12} - C_{13} - C_{23}}{15} \quad (7)$$

and Reuss approximation [62] as given below;

$$B_R = \frac{1}{S_{11} + S_{22} + S_{33} + 2(S_{12} + S_{13} + S_{23})} \quad (8)$$

$$G_R = \frac{15}{4(S_{11} + S_{22} + S_{33}) - 2(S_{12} + S_{13} + S_{23}) + 3(S_{44} + S_{55} + S_{66})} \quad (9)$$

where $S_{ij} = (C_{ij})^{-1}$ represents the elastic compliance constants. The effective bulk B and shear modulus G is obtained by taking arithmetic average of Voigt and Reuss bulk (B_V and B_R) and shear (G_V and G_R) modulus by means of Hill's approximation [63];

$$B = \frac{B_V + B_R}{2} \quad (10)$$

$$G = \frac{G_V + G_R}{2} \quad (11)$$

Young's modulus E and the Poisson's ratio ν are calculated from the relations given below;

$$E = \frac{9BG}{3B + G} \quad (12)$$

$$\nu = \frac{3B - 2G}{2(3B + G)} \quad (13)$$

The calculated Voigt, Reuss, Hill bulk modulus (B_V, B_R, B), shear modulus (G_V, G_R, G), Young's modulus (E), B/G ratio, Poisson ratio (υ), bulk modulus along a-, b-, and c-axis (Ba, Bb, Bc) and anisotropic factors (Aa, Ac) of the XAl_2O_4 (X = Ca, Sr and Cd) compounds are tabulated in Table 4. The calculated bulk modulus (B) for the $CaAl_2O_4$ compound compared to the available experimental and theoretical studies in the literature deviate by about 19.02% [26-Exp.] and 2.48% [26], respectively. There is not any data for $SrAl_2O_4$ and $CdAl_2O4$ compounds in literature to compare our results. Taking into account the calculated results for structural parameters including elastic constants given in Tables 3 and 4, we can make following conclusions;

i. Bulk modulus B represents the resistance against the change in the volume with pressure. B of the examined compounds descent in the order of $CdAl_2O_4 > CaAl_2O_4 > SrAl_2O_4$.
ii. The shear modulus G makes it possible to resist the deformation of the solid state materials due to the shear force. G values have the following relation; $CaAl_2O_4 > CdAl_2O_4 > SrAl_2O_4$ for the studied compounds. Therefore we can conclude that $CaAl_2O_4$ has the highest hardness while $SrAl_2O_4$ has the lowest one.
iii. Resistance to implemented stress and strain and the stiffness of the solid state materials can be determined by Young's modulus E. So that the higher the Young's modulus, the stiffer the material. Young's modulus of the studied materials decreases in the sequence $CaAl_2O_4 > CdAl_2O_4 > SrAl_2O_4$. It is clear that $CaAl_2O_4$ is more stiffer than the other compounds studied in this paper.
iv. The ratio of bulk modulus and shear modulus B/G gives insight into the ductile and brittle nature of the solid material [64]. Studied materials is ductile if $B/G > 1.75$ and brittle if $B/G < 1.75$. In the present study (see Table 4), it can be clearly seen that $CaAl_2O_4$ and $SrAl_2O_4$ are brittle whereas $CdAl_2O_4$ is ductile in nature.
v. The brittle and ductile nature of any crystal can also be determined by Cauchy's pressure using Pettifor's rule [65] which states that if the materials have more metallic bonds then the materials are ductile. On the contrary, if the materials have more angular bonds then the materials are brittle in nature. For the materials having orthorhombic structure, the Cauchy pressures along {100}, {010} and {001} planes are (C_{23}–C_{44}), (C_{13}–C_{55}) and (C_{12}–C_{66}), respectively. In the present study, the calculated Cauchy pressure along {100} plane is −35.58 GPa, −13.33 GPa and −1.92 GPa, along {010} plane is −12.57 GPa, 4.45 GPa and 36.42 GPa, along {001} plane is −41.71 GPa, −28.06 GPa and 16.34 GPa for $CaAl_2O_4$, $SrAl_2O_4$ and $CdAl_2O_4$ compounds, respectively.

Table 4
The calculated Voigt, Reuss, Hill bulk modulus (B_V, B_R, B in GPa), shear modulus (G_V, G_R, G in GPa), Young's modulus (E in GPa), B/G ratio, Poisson ratio (υ), bulk modulus along a-, b-, and c-axis (B_a, B_b, B_c in GPa) and anisotropic factors (A_a, A_c) for XAl_2O_4 (X = Ca, Sr and Cd).

Pnma	$CaAl_2O_4$	$SrAl_2O_4$	$CdAl_2O_4$
B_V	181.79	164.18	192.40
B_R	180.97	162.02	191.51
B	181.38	163.10	191.96
	224 [26-Exp.]		
	186 [26]		
G	126.12	103.50	103.65
G_V	127.04	105.90	105.27
G_R	125.19	101.09	102.03
E	307.16	256.28	263.53
B/G	1.44	1.58	1.85
υ	0.2178	0.2381	0.2712
B_a	257.46	386.25	471.96
B_b	332.51	766.00	604.99
B_c	403.04	447.00	560.26
A_a	0.7743	0.5043	0.7785
A_c	1.2121	0.5836	0.9261

For the $CaAl_2O_4$ compound, the bonding in the {100}, {010} and {001} planes have metallic character while in the case of $SrAl_2O_4$ compound, the bonding along the planes {100} and {001} have metallic character and the bonding along the plane {010} have angular character. The results show that the bonding in the $CdAl_2O_4$ compound have angular character along {100} plane and metallic character along the {010} and {001} planes. For the $CaAl_2O_4$ compound, the bonding in the {100}, {010} and {001} planes have angular character while in the case of $SrAl_2O_4$ compound, the bonding along the planes {100} and {001} have angular character and the bonding along the plane {010} have metallic character.

The elasticity and shape of any crystal is directly related to its elastic constants. In Table 3, it is observed that the elastic constant C_{22} is greater than the elastic constants C_{11} and C_{33}, thus these compounds are anisotropic in nature. The elastic anisotropy of the orthorhombic crystal can be defined by bulk modulus B_a, B_b and B_c along a-, b- and c-axis, respectively [66] and these are related as;

$$B_a = a\frac{dP}{da} = \frac{\chi}{1+\alpha+\beta} \tag{14}$$

$$B_b = b\frac{dP}{db} = \frac{B_a}{\alpha}, \tag{15}$$

$$B_c = c\frac{dP}{dc} = \frac{B_a}{\beta} \tag{16}$$

where,

$$\chi = C_{11} + 2C_{12}\alpha + C_{22}\alpha^2 + 2C_{13}\beta + C_{33}\beta^2 + 2C_{23}\alpha\beta, \tag{17}$$

$$\alpha = \frac{(C_{11}-C_{12})(C_{33}-C_{13}) - (C_{23}-C_{13})(C_{11}-C_{13})}{(C_{33}-C_{13})(C_{22}-C_{12}) - (C_{13}-C_{23})(C_{12}-C_{23})}, \tag{18}$$

$$\beta = \frac{(C_{22}-C_{12})(C_{11}-C_{13}) - (C_{11}-C_{12})(C_{23}-C_{12})}{(C_{22}-C_{12})(C_{33}-C_{13}) - (C_{12}-C_{23})(C_{13}-C_{23})} \tag{19}$$

The calculated values of the bulk modulus along *a*-, *b*- and *c*-axis are listed in Table 4. It is clear from Table 4 that B_b is much greater than the B_a and B_c for $CdAl_2O_4$ and $SrAl_2O_4$ while for $CaAl_2O_4$, B_c is much greater than B_a and B_b. This means that the $CdAl_2O_4$ and $SrAl_2O_4$ compounds are less compressible along *b*-axis in comparison to *a*- and *c*-axis while $CaAl_2O_4$ is less compressible along *c*-axis in comparison to the *a*- and *b*-axis.

The anisotropy in the bulk modulus along *a*- and *c*-axis with respect to *b*-axis is represented as;

$$A_a = \frac{B_a}{B_b} = \alpha, \tag{20}$$

$$A_c = \frac{B_c}{B_b} = \frac{\alpha}{\beta} \tag{21}$$

Crystal is isotropic if the values of A_a and A_c are 1 and any deviation from zero indicates the anisotropic nature of the crystal. In the present study, the calculation shows that the bulk modulus of the studied XAl_2O_4 (X = Ca, Sr and Cd) compounds are anisotropic in nature.

Obtained elastic constants can be used as input data to calculate the shear anisotropy factor along the planes {100}, {010} and {001} as $A_{\{100\}}$, $A_{\{010\}}$ and $A_{\{001\}}$, respectively, with the relations [66] given below;

$$A_{\{100\}} = \frac{4C_{44}}{C_{11}+C_{33}-2C_{13}}, \tag{22}$$

$$A_{\{010\}} = \frac{4C_{55}}{C_{22}+C_{33}-2C_{23}}, \tag{23}$$

$$A_{\{100\}} = \frac{4C_{66}}{C_{11}+C_{22}-2C_{12}}, \tag{24}$$

If the values of $A_{\{100\}}$, $A_{\{010\}}$ and $A_{\{001\}}$ are equal to 1 then the crystal is isotropic in nature and if there is a deviation from unity then the crystal is anisotropic in nature. The calculated shear anisotropy factors *A*{100}, *A*{010} and *A*{001}, percentage anisotropy factors of bulk A_B and shear modulus A_G and universal anisotropy factor A^U of the XAl_2O_4 (X = Ca, Sr and Cd) compounds are tabulated in Table 5. According to given results in Table 5, these compounds show shear anisotropy. The results also show that there is a large deviation from absolute value along {001} for $CdAl_2O_4$ and $CaAl_2O_4$ and along {100} for $SrAl_2O_4$. This means that the shear anisotropy has a greater value along {001} for $CdAl_2O_4$ and $CaAl_2O_4$ and along {100} for $SrAl_2O_4$.

Table 5
The calculated values of shear anisotropy factors $A_{\{100\}}$, $A_{\{010\}}$ and $A_{\{001\}}$, percentage anisotropy factors of bulk A_B and shear modulus A_G and universal anisotropy factor A^U for XAl_2O_4 (X = Ca, Sr and Cd).

Compound	$A_{\{100\}}$	$A_{\{010\}}$	$A_{\{001\}}$	A_B	A_G	A^U
$CaAl_2O_4$	1.1516	0.8800	0.7574	0.2262	0.7316	0.0782
$SrAl_2O_4$	1.6186	1.0564	0.8363	0.6625	2.3194	0.2508
$CdAl_2O_4$	1.0899	0.7082	0.6570	0.2320	1.5635	0.1635

The percentage of anisotropy factor from bulk modulus (A_B) and shear modulus (A_G) for the orthorhombic crystal can be calculated by the relation given by Chung and Buessem [67];

$$A_B = \frac{B_V - B_R}{B_V + B_R} \times 100\%, \tag{25}$$

$$A_G = \frac{G_V - G_R}{G_V + G_R} \times 100\% \tag{26}$$

The calculated values of A_B and A_G are listed in Table 5 which shows that the value of A_G is significantly larger than the value of A_B for all the studied compounds $CaAl_2O_4$, $SrAl_2O_4$ and $CdAl_2O_4$. This means that the studied compounds in this paper show a small anisotropy in bulk modulus but a high anisotropy in shear modulus.

The universal anisotropy factor (A^U) is also a measure of the anisotropic properties of the crystals as [68];

$$A^U = \frac{5G_V}{G_R} + \frac{B_V}{B_R} - 6 \geq 0 \tag{27}$$

If $A^U = 0$ crystal is isotropic and any deviation from absolute value shows the anisotropic nature of the crystal. The universal anisotropy for studied compounds have been calculated and results are given in Table 5. From Table 5 it is obvious that the studied compounds are highly anisotropic in nature.

The specific heat and melting temperature are closely related to the Debye temperature (θ_D). Acoustic vibrations are only responsible for the vibrations of the crystals at low temperatures. Therefore using the elastic constants as input, Debye temperature at low temperature values can be calculated using the relations [69];

$$\theta_D = \frac{\hbar}{k}\left[\frac{3n}{4\pi}\left(\frac{N_A\rho}{M}\right)\right]^{1/3} \nu_m \tag{28}$$

where ħ is the Planck's constants divided by 2π, *k* is Boltzmann's constant, N_A is Avogadro's number, *n* is the number of atoms per formula unit, *M* is the molecular mass per formula unit, ρ is the density and ν_m is the average sound velocity given by the following formula [70];

$$\nu_m = \left[\frac{1}{3}\left(\frac{2}{\nu_t^3} + \frac{1}{\nu_l^3}\right)\right]^{-1/3} \tag{29}$$

where ν_t is the longitudinal and ν_l is the transverse elastic wave velocities. The longitudinal and transverse elastic velocities can be calculated by using the relation given below as [71];

$$\nu_l = \sqrt{\frac{3B+4G}{3\rho}} \quad \text{and} \quad \nu_m = \sqrt{\frac{G}{\rho}} \tag{30}$$

The calculated values of density, longitudinal, transverse, average sound velocities and Debye temperature of the studied

Table 6
Density (ρ in g/cm^3), longitudinal, transverse and average velocities (in m/s) and Debye temperature (Θ_D in K) for XAl_2O_4 (X = Ca, Sr and Cd).

Compound	ρ	v_l	v_t	v_m	θ_D	Ref.
$CaAl_2O_4$	3.864	9509	5712	6318	882.0	Present
	3.58	–	–	–	–	[21-Exp.]
	3.975	–	–	–	–	[22-Exp.]
	–	–	–	–	831	[23-Exp.]
	3.973	–	–	–	–	[24-Exp.]
	3.97	–	–	–	–	[26-Exp.]
	3.89	–	–	–	–	[26]
	3.86	–	–	–	–	[28]
$SrAl_2O_4$	4.655	8039	4713	5225	711.2	Present
$CdAl_2O_4$	5.607	7673	4299	4785	667.0	Present

compounds are tabulated in Table 6 along with the available results in literature. It is well known that the higher the Debye temperature the higher the microhardness of the materials. Table 6 shows that the orthorhombic $CaAl_2O_4$ have the highest Debye temperature among the other studied compounds. Thus, it has higher microhardness compared to other compounds. The microhardness of the studied compounds has the sequence of $CaAl_2O_4 > SrAl_2O_4 > CdAl_2O_4$. Besides, Kojitani et al. [23] have experimentally measured the heat capacity of $CaAl_2O_4$ calcium ferrite using a differential scanning calorimeter (DSC). In this manner, Debye temperature (831 K) of calcium ferrite type $CaAl_2O_4$ has been derived from the heat capacity. The computed Debye temperature is compatible with the value reported by them. Besides, the calculated density (ρ) for $CaAl_2O_4$ is in good agreement with Refs. [21,22,24,26,28]. There is not any reference data for longitudinal, transverse and average sound velocities of the investigated compounds. All the obtained elastic calculations for $SrAl_2O_4$ and $CaAl_2O_4$ compounds with the orthorhombic phase need to be verified experimentally since we do not have any literature information to compare our results.

3.3. Electronic properties

The electronic properties, partial and total electronic density of states of the $CaAl_2O_4$, $SrAl_2O_4$ and $CdAl_2O_4$ compounds have been calculated and related graphs are plotted along high symmetry directions as shown in Figs. 2–4, respectively. From these figures it can be seen that there is a direct band gap of 4.86, 4.54 and 2.46 eV for $CaAl_2O_4$, $SrAl_2O_4$ and $CdAl_2O_4$ compounds, respectively. Furthermore, when the calculated direct band gap values for these compounds are examined, it is clear that these values are arrayed as E_g ($CaAl_2O_4$)> E_g ($SrAl_2O_4$)> E_g ($CdA1_2O_4$) depending on the displacement of the X atom. Namely, the band gap values decreases in XAl_2O_4 compounds as X atom goes from Ca to Sr, Cd. The maximum of the valence with the minimum of the conduction band are at Γ symmetry point for these compounds. Thus they are direct band gap semiconductors. Our calculated band gap value for $CaAl_2O_4$ compound is in good agreement with the band gap (4.9 eV) obtained in Ref. [27] and (4.85 eV) in Ref. [28]. There are no studies on the electronic properties of other compounds for *Pnma* phase.

From the partial density of states for the $CaAl_2O_4$ and $SrAl_2O_4$ compounds (Figs. 2 and 3), it can be concluded that the valence band of these compounds are formed mainly by the contribution of p orbitals of O atom and small contributions of d and p orbitals of Ca (Sr) atom and p orbitals of Al atoms. And the contributions of the rest of the orbitals of the constituent atoms are negligibly small. From Figs. 2 and 3, it is also seen that the contributions of the p orbitals of O atom increases as we move from bottom of the valence band to the fermi surface. The conduction band of the $CaAl_2O_4$ and $SrAl_2O_4$ compounds is mainly formed by the contributions of the d orbitals of Ca (Sr) atoms, small contributions of p orbitals of O atom and negligibly small contributions of the rest of the orbitals of the constituent atoms.

The partial density of states (Fig. 4) of the $CdAl_2O_4$ compound shows that the valence band between the energy range (−6 eV and 0 eV) is mainly constructed by the contribution of the p orbitals of O atoms and the small contribution of the d orbital of Cd atoms. However the contributions of the rest of the orbitals of the Cd, Al and O atoms are insignificantly small. It also seems that the contributions of the p orbitals of O atoms increase and the contribution of the d orbital of Cd atom decreases with the increase in the energy of the valence band. On the other hand, the construction of conduction band is mainly due to the contributions of the p orbitals of the Cd atoms and O atoms. However, the contributions of rest of the orbitals of the constituent atoms are negligibly small in conduction band.

3.4. Vibrational properties

The orthorhombic XAl_2O_4 (X = Ca, Sr and Cd) compounds have *Pnma* space group. The unit cell of XAl_2O_4 (X = Ca, Sr and Cd) with

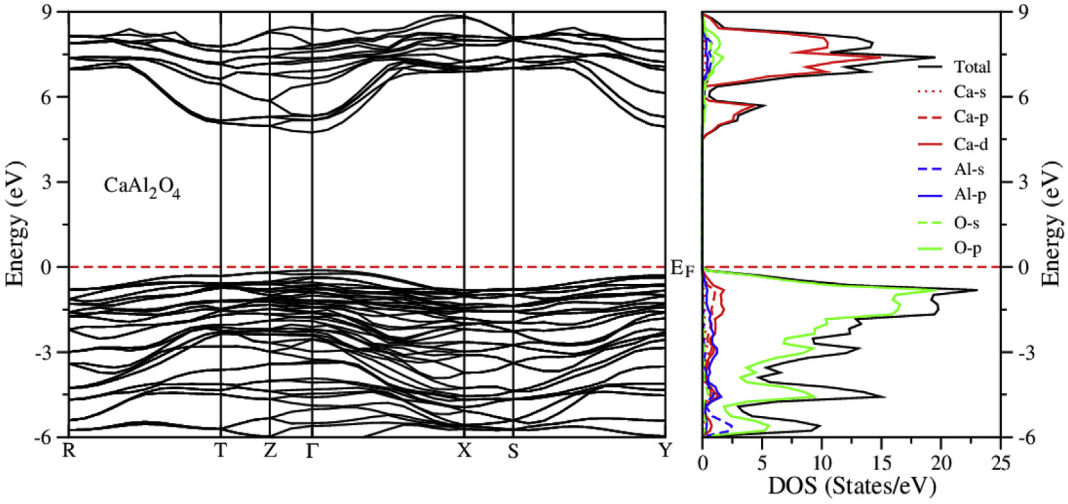

Fig. 2. (Colour online) Electronic band structure, total and partial density of states for $CaAl_2O_4$. (For interpretation of the references to color in this figure legend, the reader is referred to the Web version of this article.)

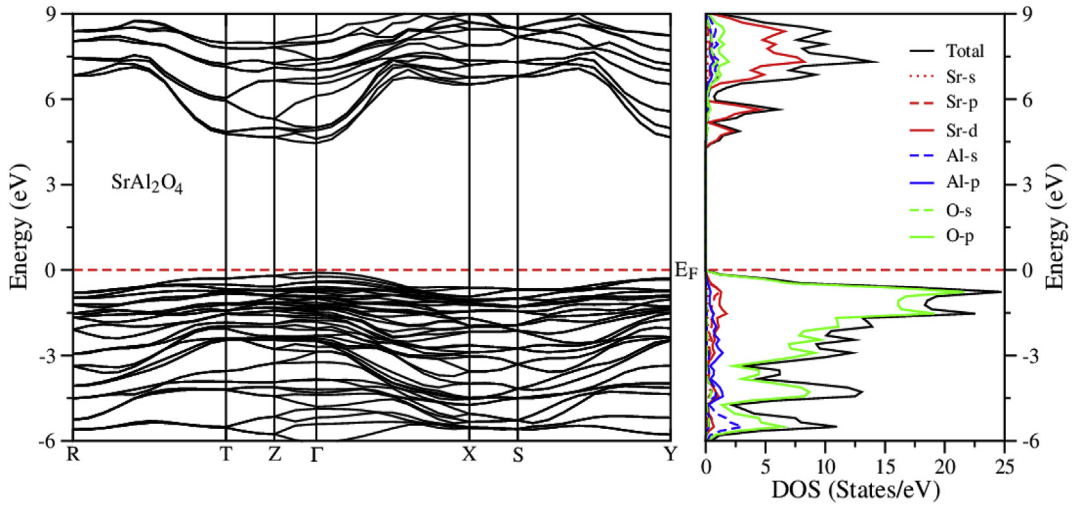

Fig. 3. (Colour online) Electronic band structure, total and partial density of states for $SrAl_2O_4$. (For interpretation of the references to color in this figure legend, the reader is referred to the Web version of this article.)

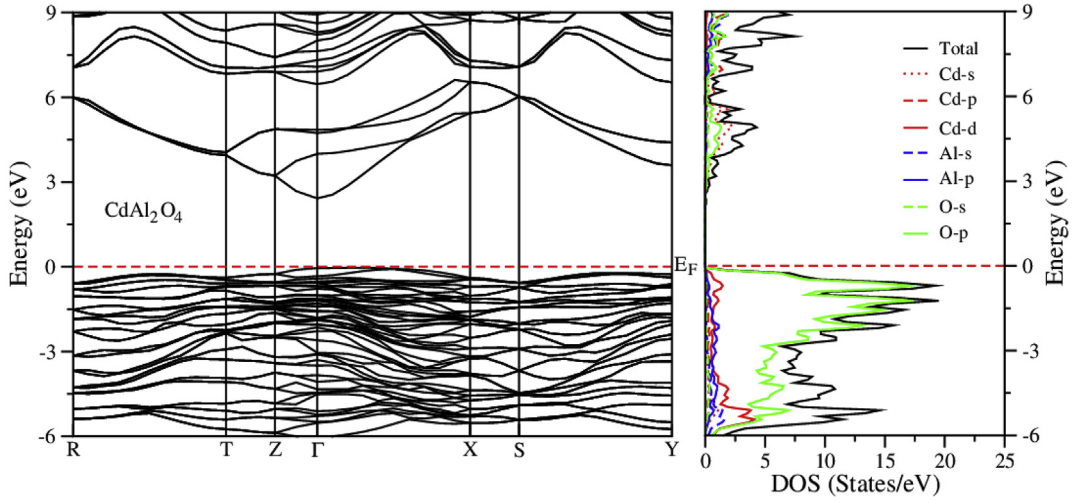

Fig. 4. (Colour online) Electronic band structure, total and partial density of states for $CdAl_2O_4$. (For interpretation of the references to color in this figure legend, the reader is referred to the Web version of this article.)

Table 7
Zone-center phonon frequencies (THz) for orthorhombic $CaAl_2O_4$.

Modes	This work	Modes	This work	Modes	This work	Modes	This work
A_u	4.181	A_g(R)	8.289	A_u	12.400	B_{1u}(I)	15.960
B_{1u}(I)	4.433	B_{1g}(R)	8.679	B_{3u}(I)	12.455	B_{3u}(I)	16.123
B_{3u}(I)	4.926	B_{1u}(I)	9.243	A_g(R)	12.542	A_g(R)	16.314
B_{1g}(R)	5.045	A_g(R)	9.431	B_{1u}(I)	12.561	B_{2g}(R)	16.703
A_u	5.151	B_{3u}(I)	9.501	B_{2u}(I)	12.569	A_g(R)	17.683
B_{3g}(R)	5.215	B_{1u}(I)	10.253	B_{3g}(R)	12.666	B_{2g}(R)	17.756
A_g(R)	5.383	B_{2g}(R)	10.385	B_{1g}(R)	12.843	A_g(R)	18.309
B_{2u}(I)	5.948	A_g(R)	10.715	A_g(R)	13.060	B_{3u}(I)	19.377
B_{3u}(I)	6.232	B_{2g}(R)	10.917	B_{3u}(I)	13.306	B_{1u}(I)	19.468
A_g(R)	6.289	B_{3u}(I)	10.962	B_{2g}(R)	13.562	B_{3u}(I)	19.913
A_u	6.390	B_{2u}(I)	11.079	A_u	13.868	B_{2g}(R)	19.977
B_{1g}(R)	6.526	A_u	11.152	B_{2u}(I)	13.922	A_g(R)	20.043
B_{2g}(R)	6.544	B_{1u}(I)	11.159	A_g(R)	14.058	B_{2g}(R)	20.254
B_{2u}(I)	6.811	B_{1g}(R)	11.226	B_{1u}(I)	14.123	B_{2g}(R)	20.540
B_{2g}(R)	6.893	B_{3g}(R)	11.282	B_{1u}(I)	14.508	B_{1u}(I)	20.546
B_{1u}(I)	7.295	B_{3u}(I)	11.307	B_{1g}(R)	14.528	A_g(R)	21.012
B_{2g}(R)	7.370	B_{2u}(I)	11.849	B_{3u}(I)	14.621	B_{1u}(I)	21.807
B_{3g}(R)	7.516	A_u	12.019	B_{3g}(R)	14.778	B_{3u}(I)	22.345
B_{3u}(I)	7.547	A_g(R)	12.035	B_{3g}(R)	15.321		
B_{3g}(R)	7.868	B_{2g}(R)	12.100	B_{1g}(R)	15.462		
B_{1u}(I)	8.284	B_{2g}(R)	12.278	B_{2g}(R)	15.641		

Table 8
Zone-center phonon frequencies (THz) for orthorhombic $SrAl_2O_4$.

Modes	This work	Modes	This work	Modes	This work	Modes	This work
$B_{1u}(I)$	2.671	$B_{3g}(R)$	7.847	$A_g(R)$	11.541	$A_g(R)$	15.744
A_u	2.993	$B_{1u}(I)$	7.973	$B_{3g}(R)$	11.605	$B_{3u}(I)$	15.886
$B_{3u}(I)$	3.282	$B_{3u}(I)$	8.012	$B_{1g}(R)$	11.637	$B_{2g}(R)$	16.089
$B_{3g}(R)$	3.559	$B_{1g}(R)$	8.502	$B_{3u}(I)$	11.872	$B_{1u}(I)$	16.101
$B_{1g}(R)$	3.563	$A_g(R)$	8.601	$B_{2g}(R)$	11.872	$A_g(R)$	16.934
$A_g(R)$	4.180	$B_{3u}(I)$	8.745	$A_g(R)$	12.461 12.490	$B_{2g}(R)$	17.010
$A_g(R)$	4.592	$B_{1u}(I)$	8.796	$B_{2u}(I)$	12.495	$A_g(R)$	17.593
$B_{2u}(I)$	4.744	$B_{2g}(R)$	8.884	$B_{3u}(I)$	12.509	$B_{3u}(I)$	18.585
$B_{2g}(R)$	4.787	$A_g(R)$	9.431	A_u	12.769	$B_{1u}(I)$	18.652
A_u	4.990	$B_{3u}(I)$	10.115	$B_{2g}(R)$	12.938	$B_{3u}(I)$	18.988
$B_{2g}(R)$	5.549	$B_{1u}(I)$	10.235	$B_{1u}(I)$	13.432	$B_{2g}(R)$	19.028
$B_{3u}(I)$	5.560	$B_{2g}(R)$	10.619	A_u	13.437	$B_{1u}(I)$	19.400
$B_{1u}(I)$	5.631	$A_g(R)$	10.812	$B_{3u}(I)$	13.461	$A_g(R)$	19.449
A_u	6.035	$B_{3g}(R)$	11.148	$B_{2u}(I)$	13.715	$B_{2g}(R)$	19.616
$B_{3u}(I)$	6.325	$B_{1g}(R)$	11.163	$B_{1u}(I)$	13.889	$A_g(R)$	19.661
$B_{2g}(R)$	6.467	A_u	11.166	$A_g(R)$	15.029	$B_{2g}(R)$	19.736
$B_{1g}(R)$	6.483	$B_{2g}(R)$	11.176	$B_{1g}(R)$	15.122	$B_{1u}(I)$	21.239
$B_{2u}(I)$	6.539	$B_{2u}(I)$	11.188	$B_{3g}(R)$	15.207	$B_{3u}(I)$	21.708
$B_{1u}(I)$	6.812	$B_{2u}(I)$	11.332	$B_{2g}(R)$	15.504		
$B_{3g}(R)$	7.287	A_u	11.402	$B_{3g}(R)$	15.539		
$A_g(R)$	7.611	$B_{1u}(I)$	11.417	$B_{1g}(R)$			

orthorhombic structure contains four formula units. The irreducible representation of crystal with *Pnma* structure at Brillouin zone center ($k = 0$) is as follows:

$$\Gamma = 13A_g + 13B_{2g} + 13B_{1u} + 13B_{3u} + 8A_u + 8B_{1g} + 8B_{3g} + 8B_{2u}(31)$$

where $13A_g$, $8B_{1g}$, $13B_{2g}$ and $8B_{3g}$ modes are Raman active, $12B_{1u}$, $7B_{2u}$ and $12B_{3u}$ modes are infrared active. One B_{1u}, one B_{2u} and one B_{3u} modes are acoustic and $8A_u$ modes are neither Raman nor infrared active therefore the A_u modes are silent modes.

The calculated zone-center phonons for orthorhombic $CaAl_2O_4$, $SrAl_2O_4$ and $CdAl_2O_4$ are collected in Tables 7–9, respectively. The calculated phonon dispersion relations along high symmetry directions as well as total and partial phonon density of states for $CaAl_2O_4$, $SrAl_2O_4$ and $CdAl_2O_4$ in orthorhombic structure are shown in Figs. 5–7, respectively. The dispersion relation shows that there is no gap between the whole spectrum and it is also found that there is no phonon frequency in the negative region. Hence we conclude that the studied $CaAl_2O_4$, $SrAl_2O_4$ and $CdAl_2O_4$ compounds are dynamically stable.

The total and projected partial density of states (Figs. 5–7) shows that in the lower energy regions the vibrations between the energy range 0–7.5 THz are mainly due to the vibrations of X atoms (X = Ca, Sr and Cd) and small contributions of Al and O atoms. It is also found that the contributions of the vibrations of Ca atom decrease and the vibrations of O and Al atoms increase with the increase in the frequency. In the case of middle frequency region between 7.5 and 17.5 THz, the vibrations are mainly due to the vibrations of O and Al atoms and the contributions of the vibrations of X atoms are insignificantly small. In the higher frequency regions where the frequency ranges are between 17.5 and 22 THz, the vibrations are mainly due to the vibrations of O atom and small contributions of the vibrations of Al atoms. The vibrations of X atoms do not take part in the vibrations of the frequency of higher energy region.

Lastly, thermodynamic properties such as specific heat and entropy, as a function of temperature for $CaAl_2O_4$, $SrAl_2O_4$ and $CdAl_2O_4$ compounds have been plotted in Fig. 8 (a) and (b). As the

Table 9
Zone-center phonon frequencies (THz) for orthorhombic $CdAl_2O_4$.

Modes	This work	Modes	This work	Modes	This work	Modes	This work
A_u	2.087	$B_{3g}(R)$	7.530	A_u	12.060 12.190	$A_g(R)$	15.574
$B_{1g}(R)$	2.328	$B_{3u}(I)$	7.540	$A_g(R)$	12.199	$B_{1u}(I)$	15.720
$B_{3g}(R)$	2.360	$B_{1g}(R)$	8.574	$B_{2g}(R)$	12.233	$B_{2g}(R)$	15.872
$B_{1u}(I)$	2.785	$B_{1u}(I)$	8.743	$B_{1u}(I)$	12.361	$B_{3u}(I)$	15.892
$A_g(R)$	3.149	$A_g(R)$	8.891	$B_{2u}(I)$	12.509	$A_g(R)$	16.540
$B_{3u}(I)$	3.178	$B_{1u}(I)$	9.112	$B_{3g}(R)$	12.644	$B_{2g}(R)$	17.300
$B_{2u}(I)$	3.366	$B_{2g}(R)$	9.246	$B_{3u}(I)$	12.673	$A_g(R)$	18.209
$A_g(R)$	3.700	$B_{2g}(R)$	10.058	$B_{1g}(R)$	12.928	$B_{2g}(R)$	18.791
$B_{2g}(R)$	3.996	$A_g(R)$	10.071	$A_g(R)$	13.276	$B_{3u}(I)$	18.828
$B_{3u}(I)$	4.116	$B_{1u}(I)$	10.076	$B_{2g}(R)$	13.422	$B_{1u}(I)$	19.184
A_u	4.402	$B_{2u}(I)$	10.191	$B_{1u}(I)$	13.609	$B_{3u}(I)$	19.595
$B_{2g}(R)$	4.502	$B_{3u}(I)$	10.280	$A_g(R)$	13.883	$A_g(R)$	19.650
A_u	5.104	A_u	10.454	A_u	13.891	$B_{2g}(R)$	19.714
$B_{1u}(I)$	5.384	$B_{3u}(I)$	10.513	$B_{2u}(I)$	14.108	$B_{1u}(I)$	19.756
$B_{2g}(R)$	5.433	$B_{1g}(R)$	10.755	$B_{3u}(I)$	14.243	$B_{2g}(R)$	20.140
$B_{1g}(R)$	5.822	$B_{3g}(R)$	10.961	$B_{1u}(I)$	14.378	$A_g(R)$	20.599
$B_{1u}(I)$	5.876	$B_{2u}(I)$	11.299	$B_{1g}(R)$	14.460	$B_{1u}(I)$	21.169
$B_{2u}(I)$	6.080	$A_g(R)$	11.434	$B_{2g}(R)$	14.756	$B_{3u}(I)$	21.722
$A_g(R)$	6.085	A_u	11.462	$B_{3g}(R)$	15.105		
$B_{3u}(I)$	6.724	$B_{2g}(R)$	11.487	$B_{3g}(R)$	15.426		
$B_{3g}(R)$	7.162	$B_{3u}(I)$	11.958	$B_{1g}(R)$			

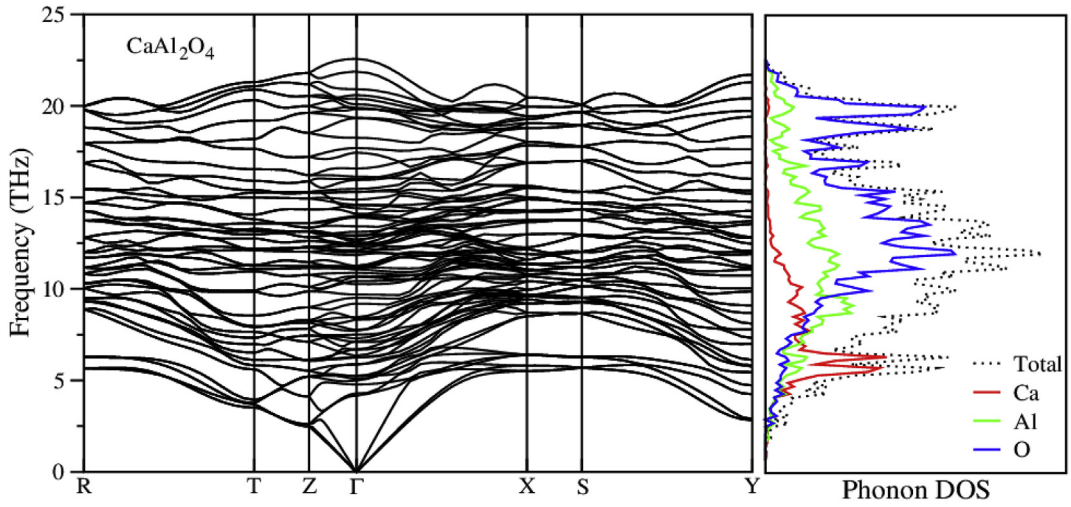

Fig. 5. (Colour online) Phonon band structure, total and partial phonon density of states for $CaAl_2O_4$. (For interpretation of the references to color in this figure legend, the reader is referred to the Web version of this article.)

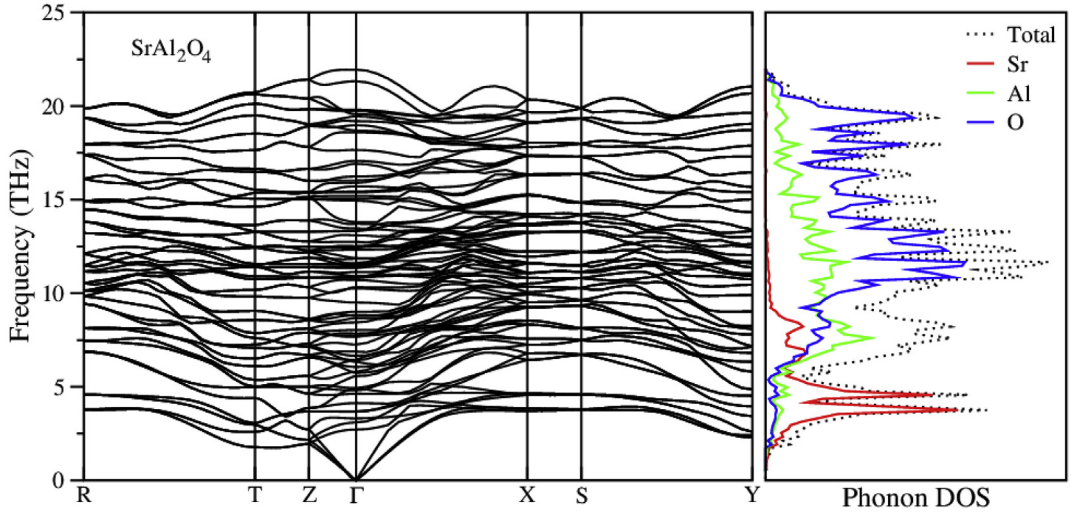

Fig. 6. (Colour online) Phonon band structure, total and partial phonon density of states for $SrAl_2O_4$. (For interpretation of the references to color in this figure legend, the reader is referred to the Web version of this article.)

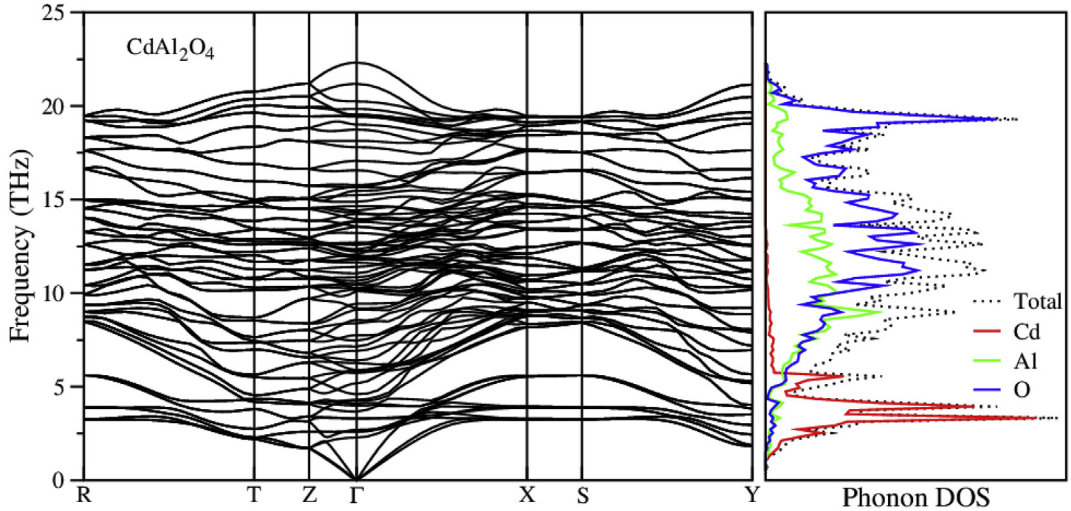

Fig. 7. (Colour online) Phonon band structure, total and partial phonon density of states for $CdAl_2O_4$. (For interpretation of the references to color in this figure legend, the reader is referred to the Web version of this article.)

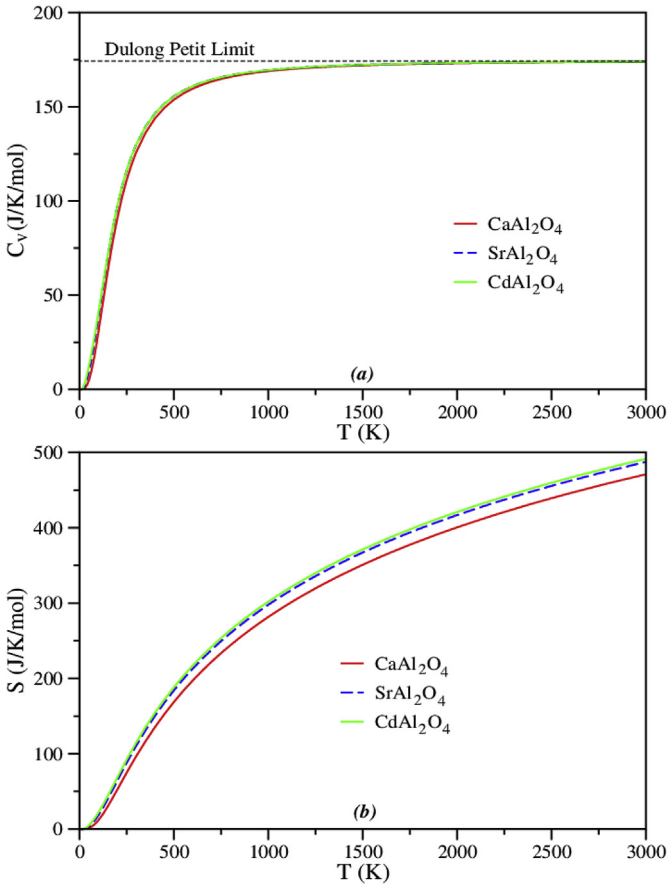

Fig. 8. (Colour online) (a) Variation of the specific heat capacity and (b) entropy at constant volume with absolute temperature for orthorhombic XAl_2O_4 (X = Ca, Sr and Cd) compounds. (For interpretation of the references to color in this figure legend, the reader is referred to the Web version of this article.)

temperature rises, the heat capacity increases quickly up to nearly 400 K and after this temperature, it goes up at a smaller rate. This correlation is fitted with the Debye temperatures as given in Table 6. The heat capacity converges to a constant known as Dulong-Petit limit [72] at high temperatures. Besides, entropy also increases with the temperature enhancement in Fig. 8 (b). Unfortunately there is no experimental and theoretical data to compare vibrational and thermodynamic properties.

4. Conclusions

In the present study, the structural, elastic, electronic and vibrational properties of orthorhombic XAl_2O_4 (X = Ca, Sr and Cd) compounds have been investigated using first-principles calculation within the generalized gradient approximation based on density functional theory. These compounds show semiconducting behavior due to their direct band gap values which makes them promising candidate for electronics application. Also, obtained direct band gap value for $CaAl_2O_4$ is in accordance with the literature. On the other hand, the obtained elastic constants show that these compounds have mechanical stability since they obey the Born-Huang criterions. Besides, Cauchy pressures show that the $CaAl_2O_4$ and $SrAl_2O_4$ compounds are ductile while the $CdAl_2O_4$ compound is brittle in nature. This agrees well with the estimation from B/G relationship. Also, the compound $CaAl_2O_4$ has more resisting power against the monoclinic shear distortion along {100} plane in comparison to $CdAl_2O_4$ and $SrAl_2O_4$. The studied compounds $CaAl_2O_4$, $SrAl_2O_4$ and $CdAl_2O_4$ are less compressible along b-axis in comparison to a- and c-axis. The elastic properties of all the studied compounds are anisotropic in nature and the $CaAl_2O_4$ compound has higher microhardness in comparison to the other two compounds. Lastly, vibrational properties are investigated and the plotted phonon dispersion curves of the studied compounds indicate that they are dynamically stable. Thermodynamic properties of these compounds have also been studied. It is observed that specific heat values get closer to Dulong-Petit limit at high temperature.

References

[1] W. Jones, L.J. Miles, Proc. Br. Ceram. Soc. 19 (1971) 161.
[2] J.M. Leger, J. Haines, M. Schmidt, J.P. Petitet, A.S. Pereira, J.A.H. Da Jordana, Nature (London) 383 (6599) (1996) 401.
[3] B.M. Mothudi, O.M. Ntwaeaborwa, S.S. Pitale, H.C. Swart, J. Alloy. Comp. 508 (2) (2010) 262–265.
[4] X. Xu, Y. Wang, Y. Li, Y. Gong, J. Appl. Phys. 105 (8) (2009), 083502.
[5] V. Singh, J.J. Zhu, M.K. Bhide, V. Natarajan, Opt. Mater. 30 (3) (2007) 446–450.
[6] T. Aitasalo, J. Hölsä, H. Jungner, M. Lastusaari, J. Niittykoski, J. Alloy. Comp. 341 (1–2) (2002) 76–78.
[7] L. Fan, X. Zhao, S. Zhang, Y. Ding, Z. Li, Z. Zou, J. Alloy. Comp. 579 (2013) 432–437.
[8] U. Rambabu, S.D. Han, Mater. Res. Bull. 48 (2) (2013) 512–520.
[9] R. Wang, J. Zhang, X. Xu, Y. Wang, L. Zhou, B. Li, Mater. Lett. 84 (2012) 24–26.
[10] F.P. Glasser, L.D. Glasser, J. Am. Ceram. Soc. 46 (8) (1963) 377–380.
[11] J.E. Iglesias, H. Steinfink, J. Solid State Chem. 6 (1) (1973) 119–125.
[12] F.R. Cruickshank, D.M. Taylor, F.P. Glasser, J. Inorg. Nucl. Chem. 26 (6) (1964) 937–941.
[13] H. Müller-Buschbaum, H.G. Schnering, Z. Anorg. Allg. Chem. 336 (5–6) (1965) 295–305.
[14] A.F. Reid, A.D. Wadsley, A.E. Ringwood, Acta Crystallogr. 23 (5) (1967) 736–739.
[15] H. Müller-Buschbaum, Z. Anorg, Allg. Chem. 343 (3–4) (1966) 113–120.
[16] S. López-Moreno, P. Rodríguez-Hernández, A. Muñoz, A.H. Romero, F.J. Manjón, D. Errandonea, E. Rusu, V.V. Ursaki, Ann. Phys. 523 (1–2) (2011) 157–167.
[17] T. Bräuniger, A.J. Hofmann, I.L. Moudrakovski, C. Hoch, W. Schnick, Solid State Sci. 51 (2016) 1–7.
[18] T. Yamanaka, A. Uchida, Y. Nakamoto, Am. Mineral. 93 (11–12) (2008) 1874–1881.
[19] X. Wang, Y. Guo, Y. Shi, A.A. Belik, Y. Tsujimoto, W. Yi, Y. Sun, Y. Shirako, M. Arai, M. Akaogi, Y. Matsushita, K. Yamaura, Inorg. Chem. 51 (12) (2012) 6868–6875.
[20] A.F. Reid, A.E. Ringwood, Earth Planet. Sci. Lett. 6 (3) (1969) 205–208.
[21] S. Ito, K. Suzuki, M. Inagaki, S. Naka, Mater. Res. Bull. 15 (7) (1980) 925–932.
[22] M. Akaogi, Y. Hamada, T. Suzuki, M. Kobayashi, M. Okada, Phys. Earth Planet. Inter. 115 (1) (1999) 67–77.
[23] H. Kojitani, K. Nishimura, A. Kubo, M. Sakashita, K. Aoki, M. Akaogi, Phys. Chem. Miner. 30 (7) (2003) 409–415.
[24] B. Lazić, V. Kahlenberg, J. Konzett, R. Kaindl, Solid State Sci. 8 (6) (2006) 589–597.
[25] B. Lazic, V. Kahlenberg, J. Konzett, Z. Kristallogr. - Cryst. Mater. 222 (2007) 690–695.
[26] N.N. Eremin, A.E. Grechanovsky, E.I. Marchenko, Crystallogr. Rep. 61 (3) (2016) 432–442.
[27] http://oqmd.org/materials/entry/21928.
[28] https://materialsproject.org/materials/mp-12441/.
[29] M. Freeda, T.D. Subash, Mater. Today: Proceedings 4 (2) (2017) 4283–4289.
[30] H. Li, S. Zhang, S. Zhou, X. Cao, Mater. Chem. Phys. 114 (1) (2009) 451–455.
[31] K.L. Scrivener, A. Capmas, Lea's Chemistry of Cement and Concrete, fourth ed., Butterworth-Heinemann, Oxford, 2003, pp. 713–782.
[32] L. Prasittisopin, I. Sereewatthanawut, J. Sustainable Cement-Based Mat. 8 (3) (2019) 180–197.
[33] H.J. Yang, K.Y. Ann, M.S. Jung, Ann. Mater. Sci. Eng. DOI:10.1155/2019/9896012.
[34] H.F.W. Taylor, Thomas Telford Publishing, London, 1997.
[35] S. Tanaka, I. Ozaki, T. Kunimoto, K. Ohmi, H. Kobayashi, J. Lumin. 87–89 (2000) 1250–1253.
[36] J.S.D. Viñuela, C.O. Areán, F.S. Stone, J. Chem. Soc., Faraday Trans. 1: Phys. Chem. In Condensed Phases 79 (5) (1983) 1191–1198.
[37] A. Bouhemadou, F. Zerarga, A. Almuhayya, S. Bin-Omran, Mater. Res. Bull. 46 (12) (2011) 2252–2260.
[38] A. Manzar, G. Murtaza, R. Khenata, M. Yousaf, S. Muhammad, Chin. Phys. Lett. 31 (6) (2014), 067401.
[39] T. Aitasalo, P. Dereń, J. Hölsä, H. Jungner, J.C. Krupa, M. Lastusaari, J. Legendziewicz, J. Niittykoski, W. Stręk, J. Solid State Chem. 171 (1–2) (2003) 114–122.
[40] M. Kowatari, D. Koyama, Y. Satoh, K. Iinuma, S. Uchida, Nucl. Instrum. Methods Phys. Res. Sect. A Accel. Spectrom. Detect. Assoc. Equip. 480 (2–3)

(2002) 431–439.
[41] A. López, M.G. Da Silva, E. Baggio-Saitovitch, A.R. Camara, R.N. Silveira, R.J.M. Da Fonseca, J. Mater. Sci. 43 (2) (2008) 464–468.
[42] X. Lin, R. Zhang, X. Tian, Y. Li, B. Du, J. Nie, Z. Li, L. Chen, J. Ren, J. Qiu, Y. Hu, Adv. Opt. Mater. 6 (7) (2018), 1701161.
[43] K.A. Gedekar, S.P. Wankhede, S.V. Moharil, R.M. Belekar, J. Adv. Ceram. 6 (4) (2017) 341–350.
[44] M. Nazarov, M.G. Brik, D. Spassky, B. Tsukerblat, A.N. Nazida, M.N. Ahmad-Fauzi, J. Alloy. Comp. 573 (2013) 6–10.
[45] Z. Fu, S. Zhou, Y. Yu, S. Zhang, Chem. Phys. Lett. 395 (4–6) (2004) 285–289.
[46] B.G. Zhai, Y.M. Huang, J. Mater. Sci. 52 (4) (2017) 1813–1822.
[47] R.E. Rojas-Hernandez, W. More, F. Rubio-Marcos, J.F. Fernandez, J. Raman Spectrosc. 50 (1) (2019) 91–101.
[48] A.K. Kushwaha, S. Akbudak, A. Candan, A.C. Yadav, G. Uğur, Ş. Uğur, Mater. Res. Express 6 (2019) 8.
[49] G. Kresse, J. Hafner, Phys. Rev. B 48 (17) (1993) 13115.
[50] G. Kresse, J. Furthmüller, Phys. Rev. B 54 (16) (1996) 11169.
[51] P.E. Blöchl, Phys. Rev. B 50 (24) (1994) 17953.
[52] G. Kresse, D. Joubert, Phys. Rev. B 59 (3) (1999) 1758.
[53] J.P. Perdew, K. Burke, M. Ernzerhof, Phys. Rev. Lett. 77 (1996) 3865.
[54] H.J. Monkhorst, J.D. Pack, Phys. Rev. B 13 (12) (1976) 5188.
[55] Y.L. Page, P. Saxe, Phys. Rev. B 65 (10) (2002), 104104.
[56] K. Parlinski, Z.Q. Li, Y. Kawazoe, Phys. Rev. Lett. 78 (21) (1997) 4063.
[57] M. Rashid, Q. Mahmood, M. Hassan, M. Yaseen, A. Laref, Phys. Scr. DOI: 10.1088/1402-4896/ab154f.
[58] S. Khawar, N.A. Noor, A. Malik, B.U. Haq, A. Laref, Mater. Res. Express 6 (8) (2019), 086308.
[59] F. Majid, S. Ata, H.M. ul Attique, A. Ali, B.U. Haq, A. Laref, Chem. Phys. Lett. 723 (2019) 44–50.
[60] M. Born, K. Huang, Dynamical Theory of Crystal Lattices, Clarendon press, 1954.
[61] W. Voigt, Lehrbuch der kristallphysik Leipzig, Teubner, 1928, p. 962.
[62] A. Reuss, Berechnung der Fließgrenze von Mischkristallen auf Grund der Plastizitätsbedingung für Einkristalle, Z. Angew. Math. Mech. 9 (1) (1929) 49–58.
[63] R. Hill, Proc. Phys. Soc. Sect. A 65 (1952) 349–354.
[64] S.F. Pugh, Lond Edinb, Dubl. Philos. Mag. 45 (367) (1954) 823–843.
[65] D.G. Pettifor, Mater. Sci. Technol. 8 (4) (1992) 345–349.
[66] P. Ravindran, L. Fast, P.A. Korzhavyi, B. Johansson, J. Wills, O. Eriksson, J. Appl. Phys. 84 (9) (1998) 4891–4904.
[67] D.H. Chung, W.R. Buessem, J. Appl. Phys. 38 (5) (1967) 2010–2012.
[68] S.I. Ranganathan, M. Ostoja-Starzewski, Phys. Rev. Lett. 101 (5) (2008), 055504.
[69] P. Wachter, M. Filzmoser, J. Rebizant, Phys. B Condens. Matter 293 (3–4) (2001) 199–223.
[70] O.L. Anderson, J. Phys. Chem. Solids 24 (7) (1963) 909–917.
[71] E. Schreiber, O.L. Anderson, N. Soga, McGraw-Hill, New York, 1973.
[72] A.T. Petit, P.L. Dulong, Recherches sur quelques points importans de la theorie de la Chaleur, 1819.